https://doi.org/10.52131/jmps.2021.0202.0017

Journal of Materials and Physical Sciences

Volume 2, Number 2, 2021, Pages 69 - 77

Journal Homepage:
https://journals.internationalrasd.org/index.php/jmps

First Principle Study of Structural, Electronic, and Optical Properties of XIn_2S_4 (X = Zn, Cd, Hg)

Jameelah Alzahrani[1], Samah Al-Qaisi[2], Q. Mahmood[1*], T. Ghrib[1]

[1] Department of physics, College of Science, Imam Abdulrahman Bin Faisal University, P.O. Box 1982, 31441, City Dammam, Saudi Arabia
[2] Palestinian Ministry of Education and Higher Education, Nablus, Palestine

ARTICLE INFO

Article History:
Received: August 20, 2021
Revised: October 18, 2021
Accepted: December 29, 2021
Available Online: December 31, 2021

Keywords:
Density Functional Theory
Electrical Conductivity
Direct Band Gap Semiconductor
Optoelectronic
Thermal Electric Efficiency

ABSTRACT

The spinel oxides are one of the prime candidates for their use in thermoelectric and optoelectronic applications. This particular article mainly deals with the thermodynamic and mechanical stabilities of spinel sulfides confirmed by formation energy and Born-mechanical stability criteria. The ductile behavior is achieved through Poisson's and Pugh's ratios. The indirect band gaps of 1.9 eV, 1.7 eV and direct band gap of 1.3 eV for $ZnIn_2S_4$, $CdIn_2S_4$ and $HgIn_2S_4$ spinel sulfides, respectively, are estimated by employing modified Becke-Johnson (mBJ) potential in the Wien2k computational program. The calculated optical characteristics such as dielectric coefficient, refractive index, absorption, reflection, energy loss coefficient and other related parametric quantities are explored to observe optoelectronic applications from UV to visible energy range as we move from Zn to Hg. Moreover, the ratios of thermal conductivity to electrical conductivity, Seebeck coefficient along with the figure of merits (ZT) are discussed to acknowledge the thermoelectric behavior of all three materials. The high values of ZT 0.84/0.74/0.79 are observed for Zn/Cd/HgIn2S4 spinel sulfides which ensure their prospective use in thermal energy conversion devices, especially in thermoelectric generators.

*Corresponding Author's Email: qmmustafa@iau.edu.sa

1. Introduction

The chemical formula of Spinals is AB_2X_4 (where A and B are most likely divalent and trivalent metallic cations, respectively), and X is an anion that forms tetrahedrons and octahedrons around A and B ions, respectively (Bragg, 1915; Nishikawa, 1915). The large variety of verified synthesis techniques for the fabrication of spinels made it feasible to tune their surface features and lattice parameters (Cheng et al., 2011; Radaelli et al., 2002), consequently, fluctuating valence states of individual atoms and their relevant compositions have demonstrated robust impact upon physical characteristics of material (Cho, Lee, Lee, Hong, & Cho, 2011; Kaczmarczyk et al., 2016; Marco et al., 2001; Sonoyama, Kawamura, Yamada, & Kanno, 2006; Zhao, Yan, Chen, & Chen, 2017). In spite of the fact that transparent conducting materials (TCM) have been proved to be valuable for diverse commercial optical applications (Brunin, Ricci, Ha, Rignanese, & Hautier, 2019), but still, traditional transparent conducting oxides (TCOs) shows complex characteristics because of the microstructures' complexity (Ginley & Bright, 2000). That's why a large part of material research community is still bus to find more efficient methods and advanced transparent conducting materials for their limitless applications in commercial optoelectronic devices. In recent years, Spinels AB_2X_4 have attracted many researchers to study the physical properties (Kefeni & Mamba, 2020; Narang & Pubby, 2021; Singh Yadav et al., 2020; Tsurkan, Krug von Nidda, Deisenhofer, Lunkenheimer, & Loidl, 2021).

A plethora of research reports is present related to the investigation of the physical properties of AB_2S_4. In 1969, $ZnIn_2S_4$ was synthesized by Range et al. The stability of cubic $ZnIn_2S_4$ spinal was ensured, even after a period of one year, no transformation from cubic to any other phase was admitted by $ZnIn_2S_4$ at room temperature and atmospheric pressure even after a period of one year (Sriram et al., 1998). The reflectivity spectra of AB_2S_4 (A=Zn, Cd and B=In, Ga) were studied for a wide energy range of 1-8eV under the action of unpolarized light at room temperature (Turowski, Kisiel, & Giriat, 1984). S. K. Batabyal et al. used the one-pot method to synthesize In_2S_3, $ZnIn_2S_4$, and $CdIn_2S_4$. Afterward, they used X-ray powder diffraction (XRPD), transmission and scanning electron microscopies (TEM & SEM), selected area electron diffraction (SAED) patterns, and energy-dispersive X-ray analysis (EDX) for the characterization purposes of nano-crystals (Batabyal, Lu, & Vittal, 2016). The effect of change in temperature on the electronic and optical properties of $HgIn_2S_4$, has been calculated for the temperature interval of 10-300 K (Syrbu, Tiron, & Zalamai, 2019). The ab-initio calculations of structural parameters, electronic properties, and transport properties were conducted by employing GGA along with SOC (spin-orbital coupling) for $HgIn_2S_4$ and $ZnIn_2S_4$ by using FP-LAPW+LO method (Kotbi, Hartiti, Fadili, Ridah, & Thevenin, 2019). The photoluminescence of $MgIn_2S_4$ and $HgIn_2S_4$ have revealed that donor-acceptor transmissions are dominant in the strong emission bands, which can also be observed in other members of this family (Fortin, Fafard, Anedda, Ledda, & Charlebois, 1991). The known physical characteristics highlighted that XIn_2S_4 (X=Zn, Cd, and Hg) can be used in various devices for commercial as well as domestic use such as; Light-emitting diodes (LED), solar cells, photocatalysis, photosensors, charge storage devices, thermoelectricity, photoconductors (Chen et al., 2016; Ling et al., 2017; Wang et al., 2021; Zhang et al., 2022).

Although, multiple reports are accessible related to the study of $ZnIn_2S_4$, $CdIn_2S_4$ and $HgIn_2S_4$ by varying X = Zn, Cd, Hg. But, as per our best knowledge, no comprehensive report is present related to the physical properties, especially the thermodynamic and detailed optical response of XIn_2S_4 (X = Zn, Cd, Hg). In this report, we present optoelectronic and thermoelectric properties of XIn_2S_4 (X = Zn, Cd, Hg) by using mBJ potential with the help of density functional theory-based calculations.

2. Method of Calculations

This work includes in-depth study of band structure, optical properties, and thermoelectric performances of XIn_2S_4 (X = Zn, Cd, Hg) spinel sulfides that have been studied by using Wien2k computational code (Peter Blaha, Schwarz, Madsen, Kvasnicka, & Luitz, 2001). In order to accurately calculate the Hamiltonian, Wien2k is built on FP-LAPW method (P Blaha & Schwarz, 1987) supported by various potentials and approximations. The Kohn-sham scheme along with PBE-GGA approximation was utilized to compute structural parameters of ground state, which was initially followed by the Murnaghan equation of state. Since PBE-GGA accurately estimates the ground-state parameters but underestimates electronic band structures. The electronic band structures are calculated by using mBJ potential (Koller, Tran, & Blaha, 2011; Tran & Blaha, 2009) to establish exact exchange and correlation with the help of following mathematical equation:

$$V_{x,\sigma}^{\mathrm{mBJ}}(r) = \mathrm{cV}_{x,\sigma}^{\mathrm{BR}}(r) + (3c-2)\frac{1}{\pi}\frac{\sqrt{5}}{12}\sqrt{\frac{2t_\sigma(r)}{\rho_\sigma(r)}} \quad (1)$$

Where $\rho_\sigma(r)$ is density of states, $V_{x,\sigma}^{\mathrm{BR}}(r)$ is Becke-Roussel (BR) potential, and c is charge convergence. The calculations for optical and thermoelectric characteristics of XIn_2S_4 (X = Zn, Cd, Hg) were followed by the electronic structures calculated with the help of mBJ potential. Kramer kroning relation (Wooten, 2013) is used to extract the optical properties in Wien2k code. While the thermoelectric properties are predicted by mean of transport coefficient in BoltzTraP code (Madsen & Singh, 2006; Scheidemantel, Ambrosch-Draxl, Thonhauser, Badding, & Sofo, 2003).

The transport distribution functions were used to obtain the Seebeck coefficient and thermoelectric conductivity as:

$$\sigma_{\alpha\beta}(\alpha,\mu) = \frac{1}{\Omega}\int \sigma_{\alpha\beta}(\varepsilon)\left[-\frac{\partial f_0(T,\varepsilon,\mu)}{\partial\varepsilon}\right]d\varepsilon \quad (2)$$

$$S_{\alpha\beta}(T,\mu) = \frac{1}{eT\Omega\sigma_{\alpha\beta}(T,\mu)} \int \sigma_{\alpha\beta}(\varepsilon)(\varepsilon-\mu)[-\frac{\partial f_0(T,\varepsilon,\mu)}{\partial\varepsilon}]d\varepsilon \quad (3)$$

Where μ, Ω, and f_0 shows the chemical potential, unit cell volume, and Fermi-Dirac distribution function respectively. In terms of BoltzTraP code, the relaxation time is 10^{-14} s. The rigid band approximation is used for evaluating the properties relative to the Fermi energy (Ryu & Oh, 2016). Moreover, the product of muffin-tin radius (R_{MT}) *and reciprocal lattice wave vector is 8. The* maximum angular momentum l_{max} is 10. G_{max} is set to 16 *(*Ry*)*$^{1/2}$*.* The K-point grid is set to 10×10×10 along with 1000 k-points, after analyzing various k-mesh orders. 35 Monk Horst-Pack k-points have been engaged for the charge/energy convergence test fixed at 0.00001 Ry, after which all three cases have shown constant energy that shows fully converged structure.

3. Results and Discussion

3.1. Thermodynamic and Mechanical Stability

Spinel sulfides XIn_2S_4 (X = Zn, Cd, Hg) are optimized in cubic phase by using PBE-GGA approximation and plotted in Fig.2. The atomic coordinates of X, In and S are (1/8, 1/8, 1/8), (1/2, 1/2, 1/2) and (1/4, 1/4, 1/4) accompanied by 227-Fd3m space group. The inter-atomic strain forces are condensed up to 0.0001 GPa to achieve more stabilized structures. The lattice constants and bulk modulus are evaluated by applying Murnaghan equation of state, summarized in Table 1. Computed lattice parameters improve from $ZnIn_2S_4$ to $HgIn_2S_4$, as well as, decay in bulk modulus have been witnessed due to varying ionic size from Zn to Hg. By using the following expression thermodynamic stability is ensured by analyzing enthalpy of formation (Mahmood et al., 2019):

$$\Delta H_f = E_{Total}(X_l In_m S_n) - lE_X - mE_{In} - nE_S \quad (4)$$

Here, $E_{Total}(X_l In_m S_n)$ expresses spinel's total energy. The bulk form energies for X (Zn, Cd, Hg), In and S are denoted by E_X, E_{In} and E_S, respectively. In all three cases the value of enthalpy is negative which divulge thermodynamically stable of considered spinal sulfides in cubic phases. Noticeable improvements have been witnessed in the enthalpy of formation by replacement of X-cations from Zn to Hg, which portray higher stability due to tetrahedral and octahedral positions that turn out to be welcoming to the cations.

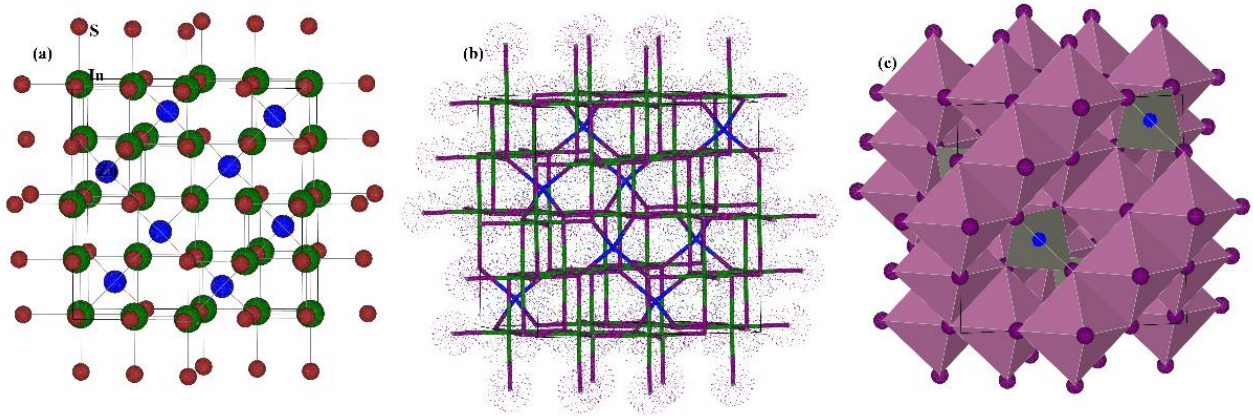

Figure 1: Computed (a) Crystal Structure, (b) Bond lengths, and (c) Polyhedral of Xin2S4 (X = Zn, Cd, Hg)

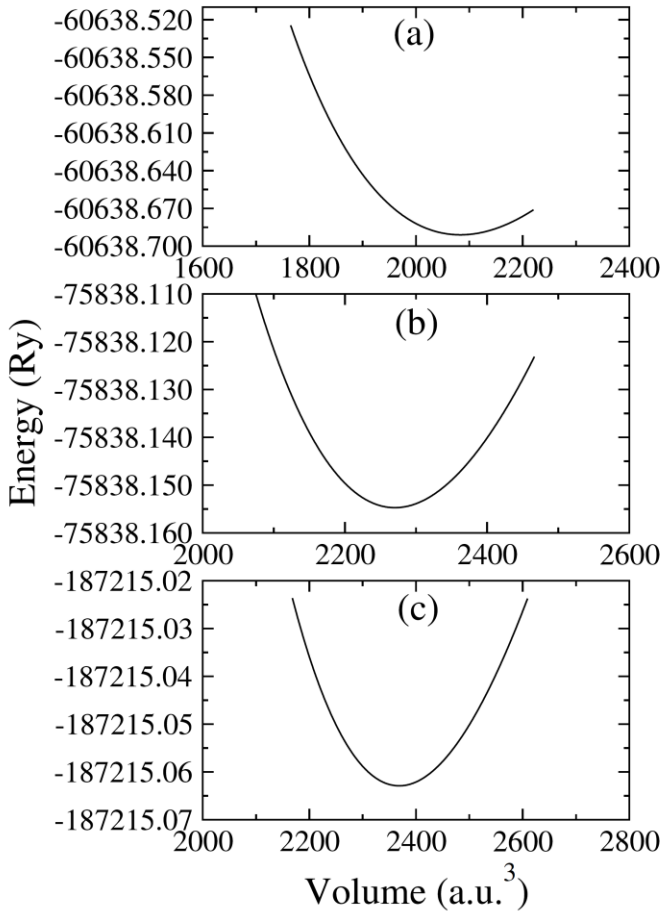

Figure 2: Optimized energy versus volume plots (a) $ZnIn_2S_4$, (b) $CdIn_2S_4$, and (c) $HgIn_2S_4$

3.2. Electronic Properties

In order to understand the electronic behavior of considered materials, the electronic band gap have been calculated by applying two well-known approximations (PBE-GGA functional and mBJ potential). The problem with PBE-GGA approximation is that it under-estimates the electronic band structure which can be resolved by using mBJ potential which improves electronic band gap as compared to the computed band gap with the help of PBE-GGA. The indirect bandgap of 1.9eV, 1.7eV and direct bandgap of 1.3eV have been visualized for ZnIn2S4, CdIn2S4 and HgIn2S4, respectively as shown in Fig.3. The decrease in bandgap with the increase in atomic radii has been observed, which ensures that electronic band gap of spinel sulfides is tunable within ultraviolet and visible energy range, which further points out to the prospect of altering the optical characteristics for range of optoelectronic devices.

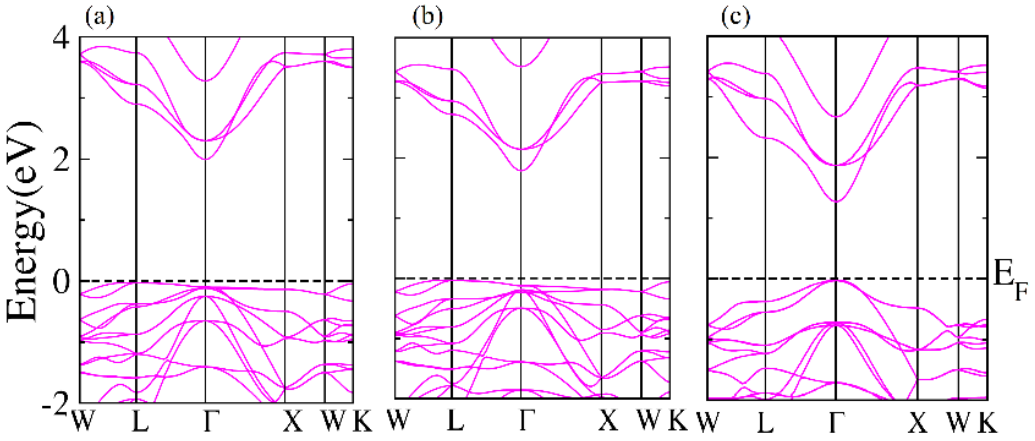

Figure 3: The band structures of (a) $ZnIn_2S_4$, (b) $CdIn_2S_4$, and (c) $HgIn_2S_4$

3.3. Optical Properties

Optical features are elaborated through interaction of light with matter, during which electrons absorb light and display inter- and intra-band electronic transitions. For optical applications purposes, the inter-band transitions are relatively more appropriate as compared to the intra-band transitions which occur within bands. Moreover, band gap of any compound has its own importance in optical behavior of any material due to the energy region having higher rate of absorption and exposure of the absorption edge (Fox, 2002; Khan, Kashyap, Solanki, Nautiyal, & Auluck, 1993; Ramay, Hassan, Mahmood, & Mahmood, 2017; Rashid et al., 2019; Zerarga, Bouhemadou, Khenata, & Bin-Omran, 2011). Several optical constraints calculated for all three materials are shown in Fig. 4(a-h). The complex dielectric constant ε(ω) = Re ε(ω) +Im ε(ω) is calculated to examine light polarization, absorption, and dispersion of incident light. The real part (Re ε(ω)) and imaginary (Im ε(ω)) parts are linked together via Kramer-Krong relation (Horsley, Artoni, & La Rocca, 2015):

$$\varepsilon_1(\omega) = 1 + \frac{2}{\pi} P \int_0^{\infty} \frac{\omega' \varepsilon_2(\omega')}{\omega'^2 - \omega^2} d\omega' \quad (5)$$

$$\varepsilon_2(\omega) = \frac{e^2 h\prime}{\pi m^2 \omega^2} \sum_{v,c} \int_{BZ}^{\infty} |M_{cv}(k)|^2 \delta[\omega_{cv}(k) - \omega] d^3k \quad (6)$$

Here P is the principal integral. The plots for Re ε(ω) are given in Fig. 4a. The static value of Re ε(ω) and calculated band gaps are in agreement with the Penn's model; Re ε(0) ≈1+ $(\hbar\omega_p/E_g)^2$, where ħ is the Planck constant and ω_p is the frequency of incident photons (Penn, 1962; Yazdanbakhsh, Khosravi, Goharshadi, & Youssefi, 2010). The maximum values of Re ε(ω) are achieved at 4.0 eV, 3.8 eV and 3.6 eV, which have shown huge variation with more increase in energy. The small humps in the energy range 5-6 eV are result of electronic transitions from occupied to unoccupied states. These values agree with stated band structures displayed in Fig. 3.

The imaginary dielectric coefficient is shown in Fig. 4b which describes the optical absorption of the considered materials. The absorption edge after which the absorption of incident photons starts to increase can be approximated with the help of the band gap. The energy of absorption edge for examined I_m ε(ω) graph agrees with relevant band gap as shown in Fig. 3. The intense peaks appeared at 4.3 eV, 4.1 eV, and 3.9 eV, for $ZnIn_2S_4$, $CdIn_2S_4$ and $HgIn_2S_4$, respectively. Therefore, maximum absorption is witnessed in UV region, that ensures their possible applicability in sterilization of surgical equipment and optoelectronics devices especially made to be used in ultraviolet region.

The refractive index *n* (*ω*), extinction coefficient *k* (*ω*) and Re ε(ω) are interrelated with each other, as stated in the equation: $n^2 - k^2 = \mathrm{Re}\varepsilon(\omega)$. The dimensionless *n* (*ω*) determine variation in the speed of light in particular material as compared to speed of light in the air and spreads wavelengths of incident light into its constituent colors, like Re ε(ω). The refractive index of transparent medium is somewhere in between 1 to 3 for visible light. Thus, the refractive indexes of these three spinels are suitable for numerous optoelectronic applications. The sharp peaks of refractive indices appear at 4.0 eV, 3.8 eV, and 3.6 eV, for $ZnIn_2S_4$, $CdIn_2S_4$, and $HgIn_2S_4$, respectively, as displayed in Fig. 4c. The displayed refractive index *n* (*0*) at zero frequency and Re ε (0) at zero frequency agrees according to the equation stated earlier, which verifies the accuracy of the computed results. The extinction coefficient and refractive index are related to the imaginary part of the dielectric coefficient by the expression; 2*nk* (*ω*) = Im ε (0) and demonstrate similarity in the behavior of extinction coefficient and Im ε(ω), as illustrated in Fig. 4d.

The absorption coefficient is calculated to visualize the absorptive nature of considered materials under the influence of incident photons passing through the particular materials is plotted in Fig. 4e. From energy value 0 eV to 1.9 eV, 1.7 eV, and 1.3 eV, for $ZnIn_2S_4$, $CdIn_2S_4$, and $HgIn_2S_4$, respectively, negligible absorption can be seen from Fig. 4e, which signify the threshold limit and is comparable to the band gaps observed from the measured band structures. The intensified rate of absorption of light occurs in UV-region as manifested earlier from Im ε(ω) and k (ω).

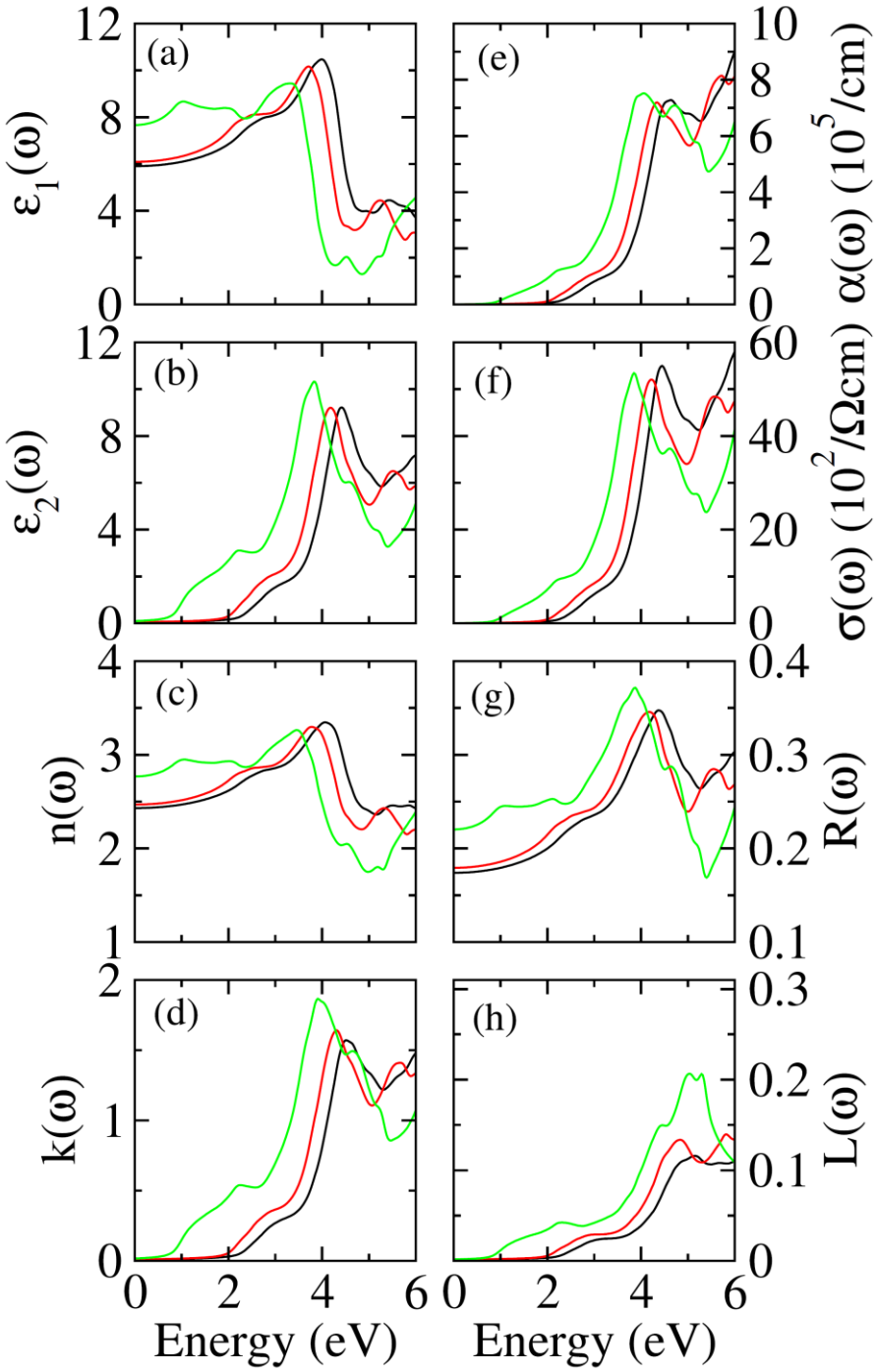

Figure 4: Computed (a) ε_1 (ω), (b) ε_2 (ω), (c) n(ω), (d) k (ω), (e) α (ω), (f) σ(ω), (g) R (ω), and (h) L (ω) for XIn_2S_4 (X = Zn, Cd, and Hg) where lines of Black, Red and Green color plots the information of $ZnIn_2S_4$, $CdIn_2S_4$ and $HgIn_2S_4$, respectively

Under the influence of light, the electrons in the valence band jumps to conduction band and generates photocurrent after sufficient energy which is required to cross the band gap energy, for that reason, optical conductivity σ (ω) of material increases with increase in the energy of incident light after the defined band gap. The computed σ (ω) are plotted in Fig. 4f, which confirms the parallel trends as seen from the absorption coefficient. The irregular behavior of the calculated reflectivity R (ω) for XIn_2S_4 (X=Zn, Cd, and Hg) is exposed in Fig. 4g. It shows high value but less than 0.4 in the energy range 3.5 eV to 4.5 eV. The energy loss L (ω) is illustrated in Fig. 4h, from which it is crystal clear that the energy loss in the visible region is very small, leading to the fact that these materials can be used for potential uses in optical device fabrication applicable in visible energy region.

4. Conclusion

This manuscript contains the detailed information about electronic, optical and thermodynamic behavior of cubic $ZnIn_2S_4$, $CdIn_2S_4$, and $HgIn_2S_4$ spinel sulfides. The negative enthalpy of formation guarantees the thermodynamic stability. The band gap is tuned from ultraviolet to visible energies by replacing Zn to Cd and Hg. $ZnIn_2S_4$ have shown maximum absorption in UV region. The overall absorption for $CdIn_2S_4$ in low energy reveals that it is a worthy choice for optoelectronic device fabrication for visible region. Furthermore, the band gap (1.3 eV) of $HgIn_2S_4$ is considered most suitable for optoelectronics. The optical loss and reflectivity are negligible in the visible region of spectrum which is ideal for optical applications.

References

Batabyal, S. K., Lu, S. E., & Vittal, J. J. (2016). Synthesis, Characterization, and Photocatalytic Properties of In2S3, ZnIn2S4, and CdIn2S4 Nanocrystals. *Crystal Growth & Design, 16*(4), 2231-2238. doi:10.1021/acs.cgd.6b00050

Blaha, P., & Schwarz, K. (1987). A full-potential LAPW study of structural and electronic properties of beryllium. *Journal of Physics F: Metal Physics, 17*(4), 899.

Blaha, P., Schwarz, K., Madsen, G. K., Kvasnicka, D., & Luitz, J. (2001). wien2k. *An augmented plane wave+ local orbitals program for calculating crystal properties, 60*.

Bragg, W. H. (1915). The Structure of Magnetite and the Spinels. *Nature, 95*(2386), 561-561. doi:10.1038/095561a0

Brunin, G., Ricci, F., Ha, V.-A., Rignanese, G.-M., & Hautier, G. (2019). Transparent conducting materials discovery using high-throughput computing. *npj Computational Materials, 5*(1), 63. doi:10.1038/s41524-019-0200-5

Chen, W., Huang, T., Hua, Y.-X., Liu, T.-Y., Liu, X.-H., & Chen, S.-M. (2016). Hierarchical CdIn2S4 microspheres wrapped by mesoporous g-C3N4 ultrathin nanosheets with enhanced visible light driven photocatalytic reduction activity. *Journal of Hazardous Materials, 320*, 529-538. doi:https://doi.org/10.1016/j.jhazmat.2016.08.025

Cheng, F., Shen, J., Peng, B., Pan, Y., Tao, Z., & Chen, J. (2011). Rapid room-temperature synthesis of nanocrystalline spinels as oxygen reduction and evolution electrocatalysts. *Nature Chemistry, 3*(1), 79-84. doi:10.1038/nchem.931

Cho, Y., Lee, S., Lee, Y., Hong, T., & Cho, J. (2011). Spinel-Layered Core-Shell Cathode Materials for Li-Ion Batteries. *Advanced Energy Materials, 1*(5), 821-828. doi:https://doi.org/10.1002/aenm.201100239

Fortin, E., Fafard, S., Anedda, A., Ledda, F., & Charlebois, A. (1991). Photoluminescence of MgIn2S4 and HgIn2S4. *Solid state communications, 77*(2), 165-167. doi:https://doi.org/10.1016/0038-1098(91)90878-Y

Fox, M. (2002). Optical properties of solids. In: American Association of Physics Teachers.

Ginley, D. S., & Bright, C. (2000). Transparent conducting oxides. *MRS bulletin, 25*(8), 15-18.

Horsley, S. A. R., Artoni, M., & La Rocca, G. C. (2015). Spatial Kramers–Kronig relations and the reflection of waves. *Nature Photonics, 9*(7), 436-439. doi:10.1038/nphoton.2015.106

Kaczmarczyk, J., Zasada, F., Janas, J., Indyka, P., Piskorz, W., Kotarba, A., & Sojka, Z. (2016). Thermodynamic Stability, Redox Properties, and Reactivity of Mn3O4, Fe3O4, and Co3O4 Model Catalysts for N2O Decomposition: Resolving the Origins of Steady Turnover. *ACS Catalysis, 6*(2), 1235-1246. doi:10.1021/acscatal.5b02642

Kefeni, K. K., & Mamba, B. B. (2020). Photocatalytic application of spinel ferrite nanoparticles and nanocomposites in wastewater treatment: Review. *Sustainable Materials and Technologies, 23*, e00140. doi:https://doi.org/10.1016/j.susmat.2019.e00140

Khan, M. A., Kashyap, A., Solanki, A. K., Nautiyal, T., & Auluck, S. (1993). Interband optical properties of ${\mathrm{Ni}}_{3}$Al. *Physical Review B, 48*(23), 16974-16978. doi:10.1103/PhysRevB.48.16974

Koller, D., Tran, F., & Blaha, P. (2011). Merits and limits of the modified Becke-Johnson exchange potential. *Physical Review B, 83*(19), 195134.

Kotbi, A., Hartiti, B., Fadili, S., Ridah, A., & Thevenin, P. (2019). Experimental and theoretical studies of CuInS2 thin films for photovoltaic applications. *Journal of*

Materials Science: Materials in Electronics, 30(24), 21096-21105. doi:10.1007/s10854-019-02479-3

Ling, C., Ye, X., Zhang, J., Zhang, J., Zhang, S., Meng, S., . . . Chen, S. (2017). Solvothermal synthesis of CdIn2S4 photocatalyst for selective photosynthesis of organic aromatic compounds under visible light. *Scientific Reports, 7*(1), 27. doi:10.1038/s41598-017-00055-5

Madsen, G. K., & Singh, D. J. (2006). BoltzTraP. A code for calculating band-structure dependent quantities. *Computer Physics Communications, 175*(1), 67-71.

Mahmood, Q., Hassan, M., Ahmad, S. H. A., Bhamu, K. C., Mahmood, A., & Ramay, S. M. (2019). Study of electronic, magnetic and thermoelectric properties of AV2O4 (A = Zn, Cd, Hg) by using DFT approach. *Journal of Physics and Chemistry of Solids, 128*, 283-290. doi:https://doi.org/10.1016/j.jpcs.2017.08.007

Marco, J. F., Gancedo, J. R., Gracia, M., Gautier, J. L., Ríos, E. I., Palmer, H. M., . . . Berry, F. J. (2001). Cation distribution and magnetic structure of the ferrimagnetic spinel NiCo2O4. *Journal of Materials Chemistry, 11*(12), 3087-3093.

Narang, S. B., & Pubby, K. (2021). Nickel Spinel Ferrites: A review. *Journal of Magnetism and Magnetic Materials, 519*, 167163. doi:https://doi.org/10.1016/j.jmmm.2020.167163

Nishikawa, S. (1915). *Proc. Tokyo Math.* Paper presented at the Phys Soc.

Penn, D. R. (1962). Wave-Number-Dependent Dielectric Function of Semiconductors. *Physical review, 128*(5), 2093-2097. doi:10.1103/PhysRev.128.2093

Radaelli, P. G., Horibe, Y., Gutmann, M. J., Ishibashi, H., Chen, C., Ibberson, R. M., . . . Cheong, S.-W. (2002). Formation of isomorphic Ir3+ and Ir4+ octamers and spin dimerization in the spinel CuIr2S4. *Nature, 416*(6877), 155-158.

Ramay, S. M., Hassan, M., Mahmood, Q., & Mahmood, A. (2017). The study of electronic, magnetic, magneto-optical and thermoelectric properties of XCr2O4 (X = Zn, Cd) through modified Becke and Johnson potential scheme (mBJ). *Current applied physics, 17*(8), 1038-1045. doi:https://doi.org/10.1016/j.cap.2017.04.011

Rashid, M., Alghamdi, A. S., Mahmood, Q., Hassan, M., Yaseen, M., & Laref, A. (2019). Optoelectronic and thermoelectric behavior of XIn2Te4 (X = Mg, Zn and Cd) for energy harvesting application; DFT approach. *Physica Scripta, 94*(12), 125709. doi:10.1088/1402-4896/ab154f

Ryu, B., & Oh, M.-W. (2016). Computational simulations of thermoelectric transport properties. *Journal of the Korean Ceramic Society, 53*(3), 273-281.

Scheidemantel, T. J., Ambrosch-Draxl, C., Thonhauser, T., Badding, J. V., & Sofo, J. O. (2003). Transport coefficients from first-principles calculations. *Physical Review B, 68*(12), 125210. doi:10.1103/PhysRevB.68.125210

Singh Yadav, R., Kuřitka, I., Vilcakova, J., Jamatia, T., Machovsky, M., Skoda, D., . . . Havlica, J. (2020). Impact of sonochemical synthesis condition on the structural and physical properties of MnFe2O4 spinel ferrite nanoparticles. *Ultrasonics Sonochemistry, 61*, 104839. doi:https://doi.org/10.1016/j.ultsonch.2019.104839

Sonoyama, N., Kawamura, K., Yamada, A., & Kanno, R. (2006). Electrochemical luminescence of rare earth metal ion doped MgIn2O4 electrodes. *Journal of the Electrochemical Society, 153*(3), H45.

Sriram, M. A., McMichael, P. H., Waghray, A., Kumta, P. N., Misture, S., & Wang, X. L. (1998). Chemical synthesis of the high-pressure cubic-spinel phase of ZnIn2S4. *Journal of materials science, 33*(17), 4333-4339. doi:10.1023/A:1004424629498

Syrbu, N. N., Tiron, A., & Zalamai, V. V. (2019). Electronic and optical properties of HgIn2S4 thiospinels. *Materials Research Express, 6*(7), 076202. doi:10.1088/2053-1591/ab17b0

Tran, F., & Blaha, P. (2009). Accurate Band Gaps of Semiconductors and Insulators with a Semilocal Exchange-Correlation Potential. *Physical Review Letters, 102*(22), 226401. doi:10.1103/PhysRevLett.102.226401

Tsurkan, V., Krug von Nidda, H.-A., Deisenhofer, J., Lunkenheimer, P., & Loidl, A. (2021). On the complexity of spinels: Magnetic, electronic, and polar ground states. *Physics Reports, 926*, 1-86. doi:https://doi.org/10.1016/j.physrep.2021.04.002

Turowski, M., Kisiel, A., & Giriat, W. (1984). Reflectivity spectra of CdIn2S4, ZnIn2S4, ZnGa2Se4and CdGa2S4. *Journal of Physics C: Solid State Physics, 17*(25), L661-L664. doi:10.1088/0022-3719/17/25/003

Wang, J., Sun, S., Zhou, R., Li, Y., He, Z., Ding, H., . . . Ao, W. (2021). A review: Synthesis, modification and photocatalytic applications of ZnIn2S4. *Journal of*

Materials Science & Technology, 78, 1-19. doi:https://doi.org/10.1016/j.jmst.2020.09.045

Wooten, F. (2013). *Optical properties of solids*: Academic press.

Yazdanbakhsh, M., Khosravi, I., Goharshadi, E. K., & Youssefi, A. (2010). Fabrication of nanospinel ZnCr2O4 using sol–gel method and its application on removal of azo dye from aqueous solution. *Journal of Hazardous Materials, 184*(1), 684-689. doi:https://doi.org/10.1016/j.jhazmat.2010.08.092

Zerarga, F., Bouhemadou, A., Khenata, R., & Bin-Omran, S. (2011). Structural, electronic and optical properties of spinel oxides ZnAl2O4, ZnGa2O4 and ZnIn2O4. *Solid State Sciences, 13*(8), 1638-1648. doi:https://doi.org/10.1016/j.solidstatesciences.2011.06.016

Zhang, G., Wu, H., Chen, D., Li, N., Xu, Q., Li, H., . . . Lu, J. (2022). A mini-review on ZnIn2S4-Based photocatalysts for energy and environmental application. *Green Energy & Environment, 7*(2), 176-204. doi:https://doi.org/10.1016/j.gee.2020.12.015

Zhao, Q., Yan, Z., Chen, C., & Chen, J. (2017). Spinels: Controlled Preparation, Oxygen Reduction/Evolution Reaction Application, and Beyond. *Chemical Reviews, 117*(15), 10121-10211. doi:10.1021/acs.chemrev.7b00051